ACS Catalysis

pubs.acs.org/acscatalysis

Research Article

Enzymatic Stetter Reaction: Computational Study of the Reaction Mechanism of MenD

Ferran Planas,* Michael J. McLeish, and Fahmi Himo*

Cite This: *ACS Catal.* 2021, 11, 12355−12366

Read Online

ACCESS | Metrics & More | Article Recommendations | Supporting Information

ABSTRACT: Quantum chemical calculations are used to investigate the detailed reaction mechanism of 2-succinyl-5-enolpyruvyl-6-hydroxy-3-cyclohexene-1-carboxylic-acid (SEPHCHC) synthase (also known as MenD), a thiamin diphosphate-dependent decarboxylase that catalyzes the formation of SEPHCHC from 2-ketoglutarate and isochorismate. This enzyme is involved in the menaquinone biosynthesis pathway in *M. tuberculosis* and is thought of as a potential drug target for anti-tuberculosis therapeutics. In addition, MenD shows promise as a biocatalyst for the synthesis of 1,4-functionalized compounds. Models of the active site are constructed on the basis of available X-ray structures, and the intermediates and transition states involved in the reaction mechanism are optimized and characterized. The calculated mechanism is in good agreement with prior kinetic studies and gives new insights into the mode of action of the enzyme. In particular, the structure and role of the tetrahedral post-decarboxylation intermediate observed in X-ray structures are discussed.

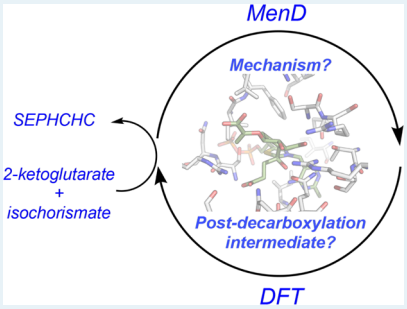

KEYWORDS: *MenD, menaquinone biosynthesis pathway, density functional theory, reaction mechanism, biocatalysis*

1. INTRODUCTION

MenD, formally known as 2-succinyl-5-enolpyruvyl-6-hydroxy-3-cyclohexene-1-carboxylic-acid (SEPHCHC) synthase, is a thiamine diphosphate (ThDP)-dependent enzyme found in the menaquinone biosynthetic pathway that has attracted interest for more than 30 years. Initially, MenD was reported to have unusual bifunctional activity, catalyzing both the 1,4-addition of 2-ketoglutarate (2KG) to isochorismate (IC) and the subsequent δ-elimination of pyruvate to form 2-succinyl-6-hydroxy-2,4-cyclohexadiene-1-carboxylate (SHCHC).[1,2] Some time later, the pyruvate elimination was shown to require a second enzyme, MenH,[3−5] and it is now accepted that the native reaction catalyzed by MenD yields only SEPHCHC (Scheme 1).

In more recent times, interest in MenD has not waned; rather, it has taken two distinct directions. First, gene knockout studies showed MenD to be essential in *B. subtilis*,[6] as well as the human pathogens *H. influenzae*[7] and *M. tuberculosis*.[8] Furthermore, it has been proposed that selective inhibition of the menaquinone biosynthesis pathway in *M. tuberculosis* may provide a novel approach to anti-tuberculosis therapeutics.[9,10] The fact that it catalyzes the first committed step in that pathway, when combined with the knockout results, has seen a number of studies focusing on the structure and mechanism of MenD as an aid to inhibitor design.

In addition to its potential as a drug target, MenD has found use as a biocatalyst due to its relatively unusual ability to catalyze 1,4-addition reactions. 1,4-Functionalized compounds have attracted interest because of their utility as synthetic intermediates,[11] but this is tempered since their preparation is challenging. One reaction that gives access to these molecules is the addition of activated aldehydes or ketoacids to α,β-unsaturated carbonyl substrates, best known as the Stetter reaction.[12] Several variations of this reaction have been developed, all based on the use of a nucleophilic catalyst to reverse the polarity of the carbonyl, thereby rendering the carbon center nucleophilic, that is, umpolung chemistry. MenD is one of a small group of enzymes termed "stetterases" that can catalyze both 1,4- and 1,2-addition reactions, the latter providing access to C4-selective chain elongation of carboxylic

Scheme 1. Reaction Catalyzed by MenD

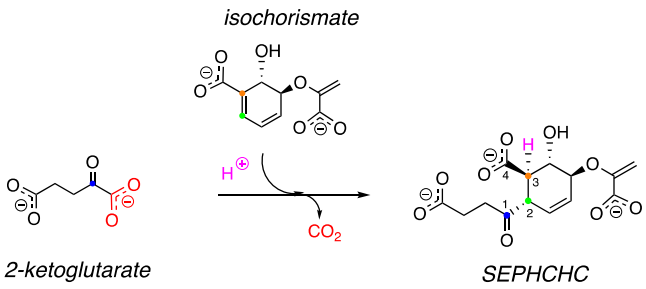

Received: May 21, 2021
Revised: August 20, 2021
Published: September 21, 2021

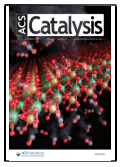

ACS Publications

© 2021 The Authors. Published by American Chemical Society

https://doi.org/10.1021/acscatal.1c02292
ACS Catal. 2021, 11, 12355−12366

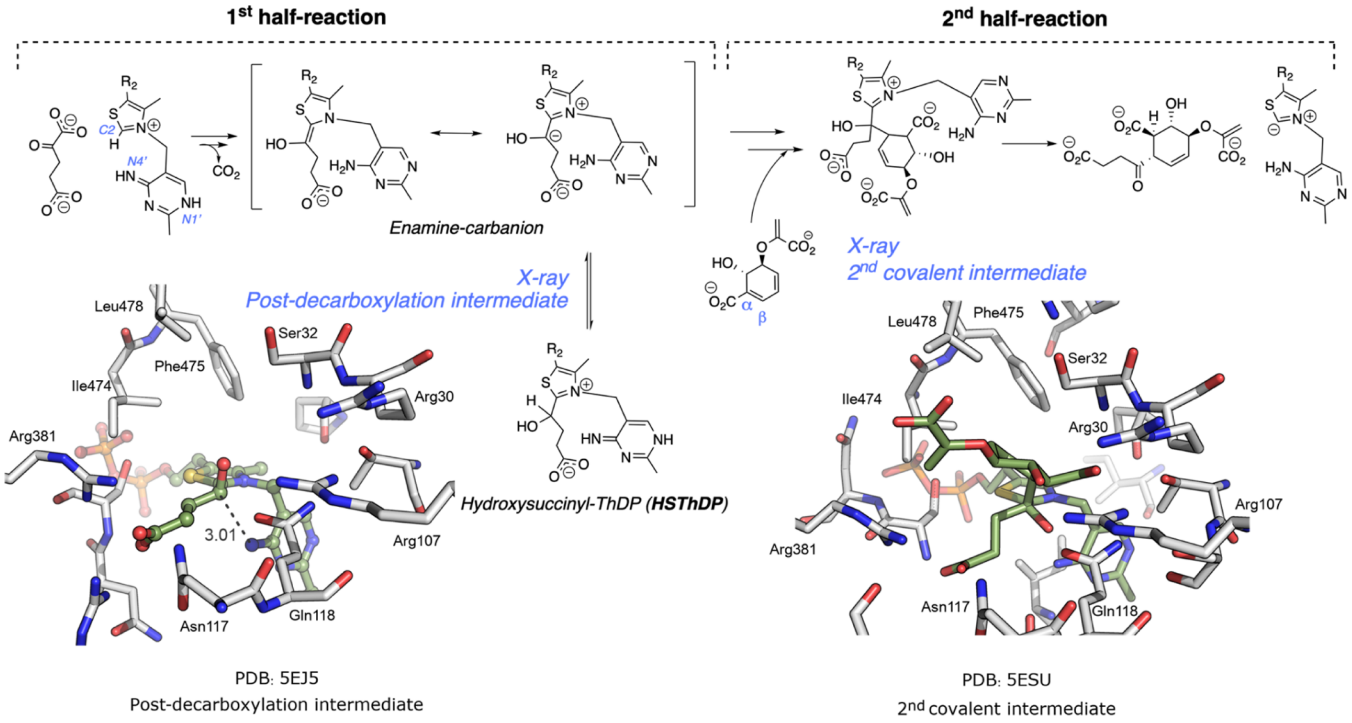

Figure 1. Proposed mechanism and observed intermediates for the MenD reaction.

substrates.[13,14] This potential industrial utility has provided additional impetus for structural and mechanistic studies of MenD.

As with those of other ThDP-dependent decarboxylases, the MenD reaction mechanism can be divided into two half-reactions: (1) the reaction of ThDP with the first or donor substrate (here, 2KG) to form a tetrahedral ThDP adduct which subsequently decarboxylates to form the Breslow (carbanion−enamine) intermediate and (2) the reaction of the Breslow intermediate with the second or acceptor substrate (here, IC) to form a second tetrahedral intermediate, which then breaks down to release the product and regenerate the cofactor (Figure 1). While most of the key aspects of the mechanism of MenD are typical, the structural studies have provided some anomalies which bear closer examination.

To date, X-ray structures have been obtained of the MenD from three sources, *B. subtilis*,[15,16] *Escherichia coli*,[17,18] and *M. tuberculosis*.[19,20] These enzymes share only ∼30% sequence identity but, typical of many ThDP-dependent enzymes, the cofactor- and substrate-binding sites of the three isozymes are virtually superimposable. Not surprisingly, the steady-state kinetic data reported for the *Bs*MenD and *Ec*MenD isozymes are also very similar.[3,16] Additional steady-state kinetics studies also revealed that MenD operates by a ping-pong mechanism in which decarboxylation of 2KG occurs prior to, and without the need for, IC binding.[21] This finding prompted experiments in which crystals of both *Ec*MenD and *Mt*MenD holoenzymes were soaked with 2KG for various time periods before being flash-frozen. X-ray analysis of the 2KG-soaked crystals revealed the development of new electron density indicative of the formation of an adduct between 2KG and ThDP. As no density was observed for the C2α carboxylate of 2KG, the adduct was assumed to be the post-decarboxylation intermediate.[17−19] In other experiments, the crystals of *Mt*MenD were also soaked with IC alone and with both 2KG and IC.[18] The former provided a structure of the holo MenD/IC complex and the latter resulted in an intermediate which was identified as the covalent donor−acceptor−ThDP adduct, commonly referred to as the second tetrahedral intermediate (Figure 1).[18]

Ultimately, soaking of the crystals with 2KG alone has provided the most intriguing of these structures. The resultant tetrahedral adduct was found in both *Mt*MenD and *Ec*MenD and was postulated to be either the carbanion or, more likely, the C2α-protonated form of the Breslow intermediate (here, **HSThDP**, Figure 1).[17,18] Unfortunately, the resolution of the X-ray structure was not sufficient to determine the exact protonation state of the intermediate but, regardless, the observation of a tetrahedral Breslow intermediate was unusual in that previously identified protonated carbanion−enamine intermediates were generally found to be planar.[22] This structure was later combined with stopped-flow and mutagenesis experiments to prompt the suggestion that MenD may operate in a novel catalytic mode, one quite distinct from the canonical enamine chemistry.[23]

Despite the plethora of X-ray structures, mutagenesis, and kinetic investigations, the MenD reaction mechanism has not been fully established. A number of questions are still open, the most important of which relates to the catalytic competence of the post-decarboxylation tetrahedral species.

We have previously used density functional theory (DFT) calculations to investigate the mechanism of the ThDP-dependent enzyme benzoylformate decarboxylase (BFDC).[24−26] In doing so, we not only established the utility of this methodology for ThDP-dependent enzymes but also, unexpectedly, were able to identify a stable yet off-pathway intermediate that had implications for the overall rate of the reaction. Here, we describe the use of the DFT methodology to investigate the reaction mechanism of MenD and show, inter alia, that it is unlikely to operate by the proposed noncanonical pathway.

https://doi.org/10.1021/acscatal.1c02292
ACS Catal. 2021, 11, 12355−12366

2. COMPUTATIONAL DETAILS

2.1. Computational Methods. All calculations were performed using the B3LYP-D3(BJ) method[27] as implemented in the Gaussian 09 package.[28] This method has been used extensively to study a wide variety of enzymatic systems.[29] For the geometry optimizations, the 6-31G(d,p) basis set was used, and the electronic energies of the stationary points were corrected by single-point calculations using the larger 6-311+G(2d,2p) basis set. These electronic energies were further refined with single-point solvation corrections using the SMD implicit solvent method[30] and a dielectric constant of $\varepsilon = 4$ and with the zero-point energy corrections, both terms calculated with the same basis set as the geometry optimizations. Following the procedure used in previous computational investigations of decarboxylating enzymes,[24,31] the entropy gain of the CO_2 release is approximated to be equal to the translational entropy of the free gas molecule (calculated to be 11.1 kcal/mol at room temperature). This value is therefore added to the energy of **Int2** (see below).

2.2. Active-Site Models. The active-site model used to study the first half-reaction was built on the basis of the X-ray structure containing the post-decarboxylation intermediate bound to MenD from *E. coli* (PDB 5EJ5). For the second half-reaction, the model was based on the X-ray structure of the donor−acceptor adduct bound to MenD from *M. tuberculosis* (PDB 5ESU), since no comparable complex with *Ec*MenD was available. This is a reasonable approach because, as noted above, the structures of the *Ec*MenD and *Mt*MenD post-decarboxylation adducts were virtually identical. In particular, superposition of the active-site residues of these structures shows minimal movements between them (see Supporting Information), in line with the least motion mechanism proposed for other ThDP-dependent enzymes.[32,33]

The same residues were included in both models (numbered according to the *E. coli* sequence): Ala29, Pro30, Gly31, Ser32, Arg33, Glu55, Thr78, Ser79, Gly80, Arg107, Asn117, Gln118, Glu172, Arg395, Arg413, Ser416, Gly417, Ile418, Ile474, Phe475, and Leu478. Two crystallographic waters, w873 and w886, were also included in the model. Of these residues, the only difference between the *Ec* and *Mt* variants are Ala29 and Ser416, which correspond to cysteine and alanine in *Mt*MenD, respectively. For the calculations reported here, Ala416 was manually mutated to Ser, while only the Cα of Ala29 is included in the model, rendering modification of Cys29 unnecessary. The X-ray structures show that the arginines in the active site are engaged in salt bridges with neighboring residues and they were therefore modeled in their protonated forms. Similarly, Glu172 was modeled in the deprotonated form to keep the salt bridge to Arg33. Glu55, which interacts with the N1′ of the cofactor, was modeled in the neutral form. However, the proton moves to the nitrogen in some steps of the mechanism (see below). The residues were truncated, as shown in Figure 2, and the atoms where the truncation is made were kept fixed at their crystallographic positions. Overall, the model for the first half-reaction comprises 319 atoms and the second half-reaction 345 atoms.

To model the first half-reaction, several different binding modes of 2KG in the enzyme−donor complex were initially considered. The reaction was then followed from the lowest-energy conformation, optimizing the subsequent transition states and intermediates along the reaction pathway. Special attention was paid to the rotatable bonds in **Int1** to identify the structure with the lowest energy. For the second half-reaction, models with several enzyme−acceptor (IC) complexes were built based on the crystal structure of the second covalent intermediate. All optimizations converged to the same geometry, reported below as **Int3**, and the reaction pathway was then followed starting from this structure.

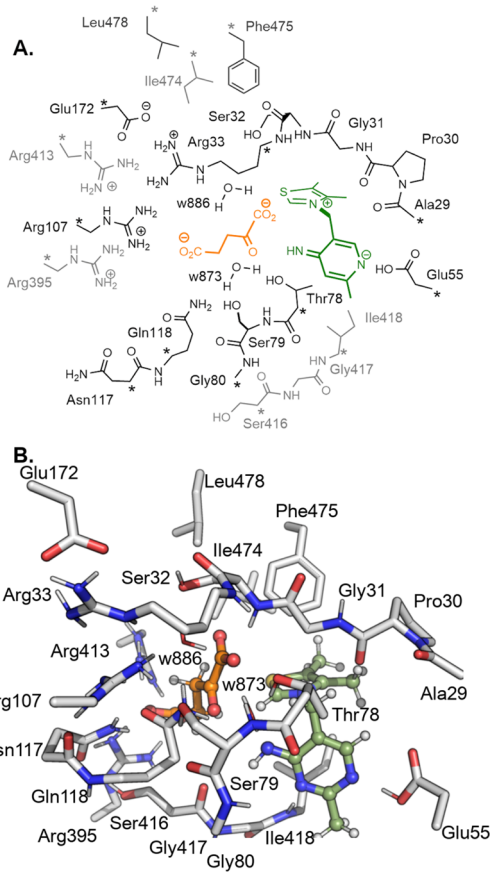

Figure 2. (A) Schematic and (B) structure of the active-site model used in this study. The asterisks indicate atoms constrained at their crystallographic positions. The cofactor is shown in green and the 2KG substrate in orange.

A final modeling point to be made here concerns the carboxylate group of the enolpyruvyl moiety of the acceptor. In the active site of *Mt*MenD, this group forms a salt bridge with an arginine residue (Arg282), an interaction that presumably is maintained in *Ec*MenD through a lysine residue (Lys292). Regardless, in both cases, the residues are remote from the donor moiety and were therefore not included in the model. Instead, the carboxylate group of the IC acceptor was modeled in the protonated form in the second-half reaction to compensate for the loss of the salt bridge.

3. RESULTS AND DISCUSSION

3.1. Initial State of the Cofactor. The ThDP cofactor can exist in a variety of forms depending on the protonation states of N1′, N4′, and C2 (Scheme 2). Moreover, two tricyclic states can also exist. As shown in our previous work on BFDC, the energies of these states depend strongly on the local environment.[24,25] In MenD, an important, and potentially consequential, consideration is that the active site does not contain any ionizable residues in the vicinity of N4′ and C2. This is highly unusual for a ThDP-dependent enzyme and, as a result, these two groups can only interact with each other.

https://doi.org/10.1021/acscatal.1c02292
ACS Catal. 2021, 11, 12355−12366

Scheme 2. Calculated Energies (kcal/mol) for the IP, TC, and YI States and the Barriers for Their Formation[a]

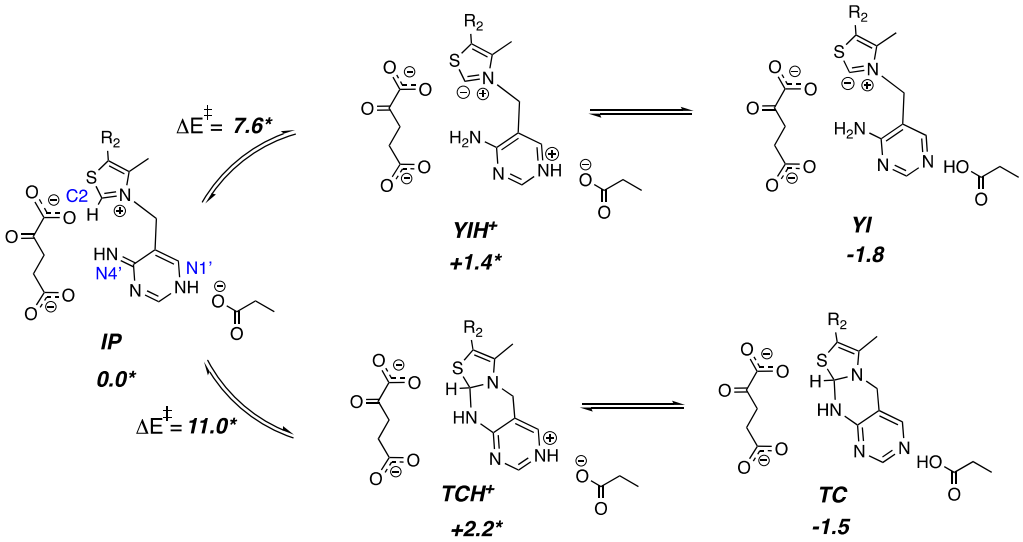

[a]The energy of **IP** is set to 0. The asterisk indicates that the N1−H bond distance was constrained in the geometry optimization of these species, see Supporting Information for discussion.

Prior to investigating the detailed reaction mechanism, it is necessary to examine the various states ThDP may adopt with the 2KG substrate bound in the MenD active site so that the most stable form of the cofactor can be identified.

We use the iminopyrimidine state (**IP**, Scheme 2) as a starting point for examining the stabilities of the various cofactor states. From here, N4′ can either extract the C2 proton to form the ylide (**YIH**$^+$) or perform an intramolecular attack on C2 to yield the catalytically unproductive tricyclic state (**TCH**$^+$). Both states can then transfer a proton from N1′ to Glu55 to form **YI** and **TC**, respectively.[25] The formation of **TCH**$^+$ is associated with a barrier of 11.0 kcal/mol, and its energy is calculated to be 2.2 kcal/mol higher than **IP** (Scheme 2). The energy of **TC** is calculated to be −1.5 kcal/mol relative to **IP**. This result is consistent with the calculated mechanism for BFDC, in which the off-cycle tricyclic species were also found to be more stable than the **IP** form.[24,25] The formation of **YIH**$^+$ is associated with a barrier of 7.6 kcal/mol relative to **IP**, and the resulting species is calculated to be +1.4 kcal/mol. On the other hand, **YI** is calculated to be −1.8 kcal/mol. Overall, we found the **YI** and **TC** forms to be of similar energies and can interconvert readily via the **IP** state.

One somewhat surprising observation from the study of MenD-bound ThDP states was that neither the energies of the ylide and tricyclic states nor the associated barriers to form these states depended significantly on the protonation state of N1′ (see Supporting Information). Likewise, the **IP** → **YI** energies calculated using a model with a protonated Glu55 and deprotonated N1′ were comparable to those obtained when the proton resided on N1′. In general, it has been established that the acid/base equilibrium established by N1′ and its vicinal glutamic acid residue (Glu55 in MenD) affects the ability of the cofactor to form the ylide that is required for catalysis.[34] However, the catalytic power of glyoxylate carboligase, a ThDP-dependent enzyme which lacks the analogous glutamic acid residue, mitigates against this being an absolute.[35]

3.2. First Half-Reaction. The reaction mechanism of MenD based on the calculations reported here is shown in Scheme 3. The associated energy profile is given in Figure 3, and optimized geometries of transition states and intermediates are displayed in Figures 4 and 5.

For this half-reaction, the Michaelis complex between the ylide (**YI**) and the donor (2KG) (Scheme 3) provides the starting point for the calculations and the energy of the complex is set to zero in Figure 3. The first catalytic step is the nucleophilic addition of the C2 of the cofactor to the carbonyl of the donor substrate. As the reaction proceeds, the developing negative charge on the C2α-alkoxide group is stabilized by hydrogen bonds with active-site water and with the N4′H_2 group of ThDP. The calculated barrier for this step is 10.6 kcal/mol (**TS1**) and the energy of the resulting tetrahedral (pre-decarboxylation) intermediate **Int1** is −6.6 kcal/mol.

Proton transfer from the N4′ of the cofactor to the C2α-alkoxide results in the formation of the **OC** species, whose energy is calculated to be 1.6 kcal/mol lower than that of **Int1**. No transition state could be located for this proton transfer, but given the short N4′H···C2αO hydrogen-bonding distance and the similar energies of **Int1** and **OC**, the barrier is expected to be very low with the two species being in rapid equilibrium. As will become apparent in the later discussion, it is significant that the cofactor in **Int1** is in the **AP** tautomer, whereas in **OC**, it adopts the **IP** tautomer, generally expected for ThDP intermediates with sp^3-hybridized C2α substituents.[34,36,37] Furthermore, the relative stability of the **OC** species is consistent with experimental investigations which suggested that protonation of the nascent alkoxide is a driving force in the formation of the ThDP−donor adduct.[38]

Previous computational studies have shown that the protonation state of N1′ can also affect the energy of the nucleophilic addition step.[39,40] Accordingly, to explore this possibility in MenD, the energy of this step was calculated using different protonation states of N1′ and Glu55. Again, as with the **IP** → **YI** transformation, we found that the energies do not change significantly (see Supporting Information).

The next step in the catalytic cycle is decarboxylation which, conceivably, could occur from either (or both) **Int1** and **OC**.

https://doi.org/10.1021/acscatal.1c02292
ACS Catal. 2021, 11, 12355−12366

Scheme 3. Mechanism of MenD Based on Calculations Described in This Work[a]

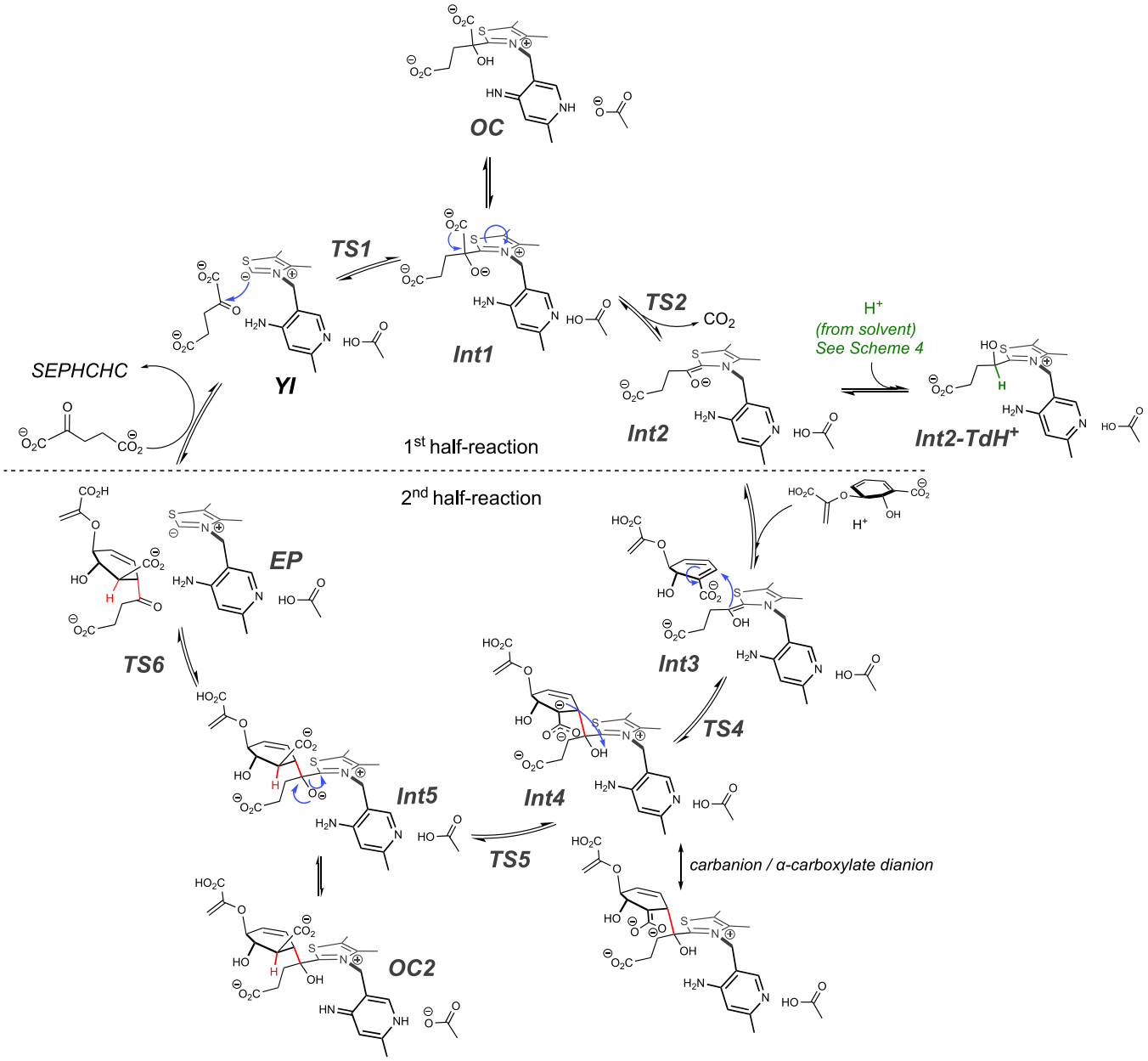

[a]Movement of electrons is highlighted in blue, while the newly formed bonds are in red.

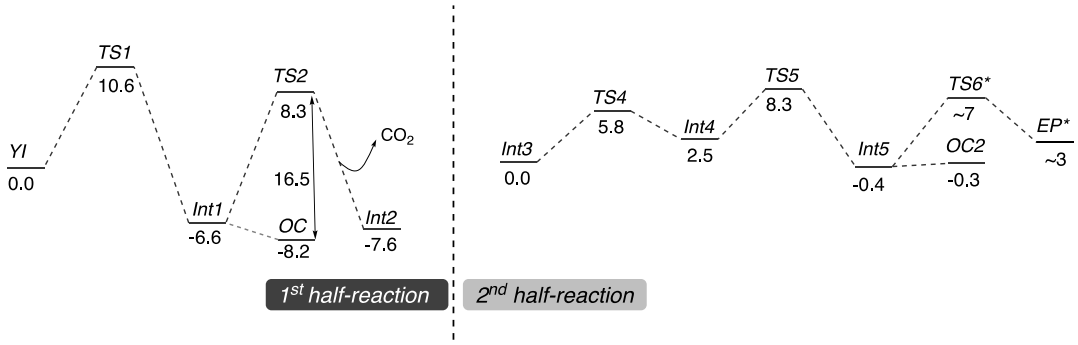

Figure 3. Calculated energy profile for the reaction mechanism starting from the Michaelis complex containing the ylide. Asterisks indicate that the energies of these structures are estimated from constrained optimizations (see text).

https://doi.org/10.1021/acscatal.1c02292
ACS Catal. 2021, 11, 12355−12366

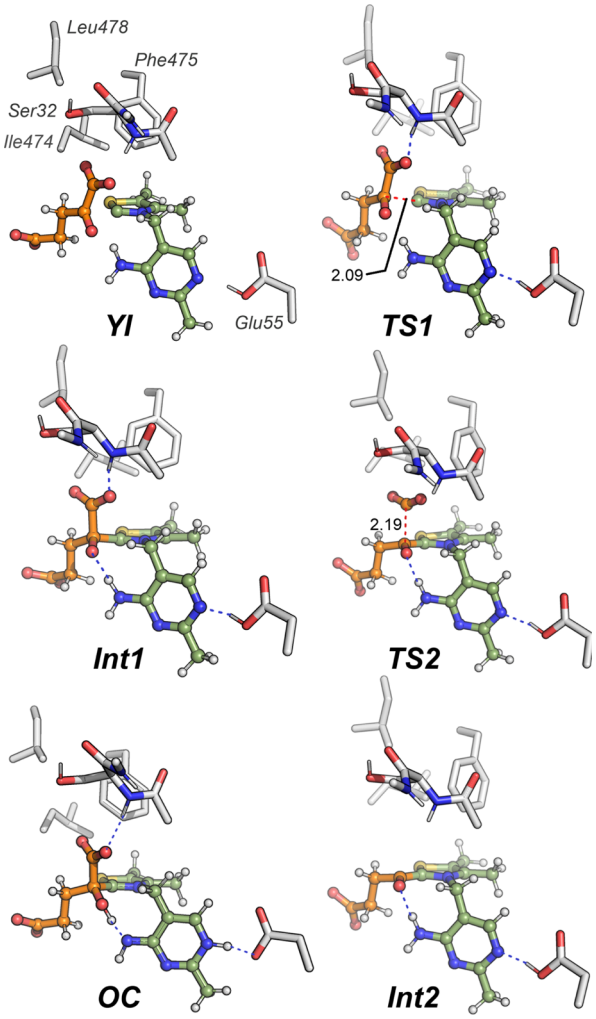

Figure 4. Optimized geometries of intermediates and transition states along the reaction pathway. For clarity, the figures show only a part of the active-site model used in the calculations.

The calculations show that decarboxylation from **OC** cannot take place, as all attempts to locate the associated transition state resulted in the deprotonation of the C2α-OH by N4′. On the other hand, decarboxylation from **Int1** is feasible and proceeds with a barrier of 14.9 kcal/mol (**TS2**) relative to **Int1**. Following the release of CO_2 from the active site, the resultant carbanion−enamine (Breslow) intermediate **Int2** is calculated to have an energy of −7.6 kcal/mol. Taken together, the calculations indicate that, even though **OC** is more stable than **Int1**, it must be considered to be an off-cycle species. Furthermore, even off-cycle, its presence effectively increases the barrier of the decarboxylation step to 16.5 kcal/mol (**OC** → **TS2**).

As described in the Introduction, soaking of MenD crystals with 2KG results in the formation of an unusual tetrahedral post-decarboxylation intermediate.[17,18] It was suggested that this arose from the transfer of a proton from N4′ of ThDP to the C2α-carbanion form of **Int2**.[17,23] Scheme 4 shows that such a transfer would produce **Int2-Td**, that is, the cofactor would be in its N4′ imino (**IP**) form. We have evaluated this possibility and found the **IP** form to be ca. 11 kcal/mol higher than **Int2**. Moreover, the associated barrier **TS-Td** is calculated to be 25.9 kcal/mol. Intriguingly, during the geometry optimization of **Int2-Td**, it was found that the C2α-alkoxide group abstracts a proton from a nearby crystallographic water molecule (w873). This implies that the energy of the **Int2** → **Int2-Td** reaction could be sensitive to the protonation state of the C2α-O group. Given also that the acidity of N4′ can potentially be affected by the protonation state of N1′,[39] we calculated the energy of the **Int2** → **Int2-Td** step using models with different protonation states of C2α-O and N1′ (see Supporting Information). Overall, the calculations show that the **Int2** → **Int2-Td** reaction is always endothermic by a minimum of 6 kcal/mol.

The relatively high energetic cost of forming **Int2-Td** is not entirely surprising as the formation of a tetrahedral post-decarboxylation ThDP intermediate previously had been found to be thermodynamically unfavorable unless the amino form could be recovered by reprotonation of N4′ by a neighboring residue.[24,41−44] Unusually, the MenD active site does not contain any ionizable residues in the vicinity of N4′ or C2α, so the recovery of the amino form requires that a proton comes from bulk solution (Scheme 4). This is true regardless of whether protonation occurs at N4′ (**Int2-Td**, **Path A**) or C2α (**Int2**, **Path B**). While conceding that the **Int2-Td** → **Int2-TdH**$^+$ energy cannot be calculated with the same accuracy as other steps in the mechanism, all estimates of the energy confirm that this process is exothermic (see Supporting Information). To ensure a comprehensive examination, one further possibility was investigated, that is, that C2αO is protonated (**Int2′**) prior to the formation of the **IP** form of the tetrahedral intermediate (**Int2-Td′**, **Path C**). This pathway was also found to be endothermic. Overall, the calculations are consistent with the formation of a stable post-decarboxylation intermediate, such as that observed in the X-ray structures, but that it will be in the **AP** rather than the **IP** form.

To continue the reaction, **Int2-TdH**$^+$ could either undergo the C2−C2α bond cleavage, which would lead to the succinic semialdehyde, or it could react with the acceptor, IC. The former is seemingly eliminated as it requires C2αO to be within the hydrogen-bonding distance of either an ionizable residue or N4′,[24,42] and these interactions are not observed in either **Int2-TdH**$^+$ or in the X-ray structures. The latter possibility is discussed in more detail in the next section.

3.3. Second Half-Reaction. The second half-reaction comprises the binding of the acceptor, IC, and the steps leading to product formation and release. Steady-state kinetic studies have shown that MenD operates by a ping-pong mechanism in which productive binding of IC does not occur until CO_2 has been released,[21] that is, IC binds to an active site in which the post-decarboxylation intermediate is already in place. What is not known is whether that intermediate will be in the planar form of a typical carbanion−enamine or in the tetrahedral form exhibited by the post-decarboxylation intermediate in the X-ray structures. To address this question, the structure of the calculated **Int2-TdH**$^+$ intermediate was superimposed on the X-ray structure of the *Mt*MenD−ThDP−IC ternary complex (PDB 5ESO[18]). It was immediately apparent that binding of the acceptor would be significantly impeded, as the C2α alkoxide (or alcohol) occupies part of the cavity in which the acceptor binds (see Supporting Information). Therefore, the only practical way for the reaction to proceed is for **Int2-TdH**$^+$ to revert to the planar **Int2**, an equilibrium process that H/D solvent exchange experiments have shown to be feasible, albeit slow, in *Ec*MenD.[17]

https://doi.org/10.1021/acscatal.1c02292
ACS Catal. 2021, 11, 12355−12366

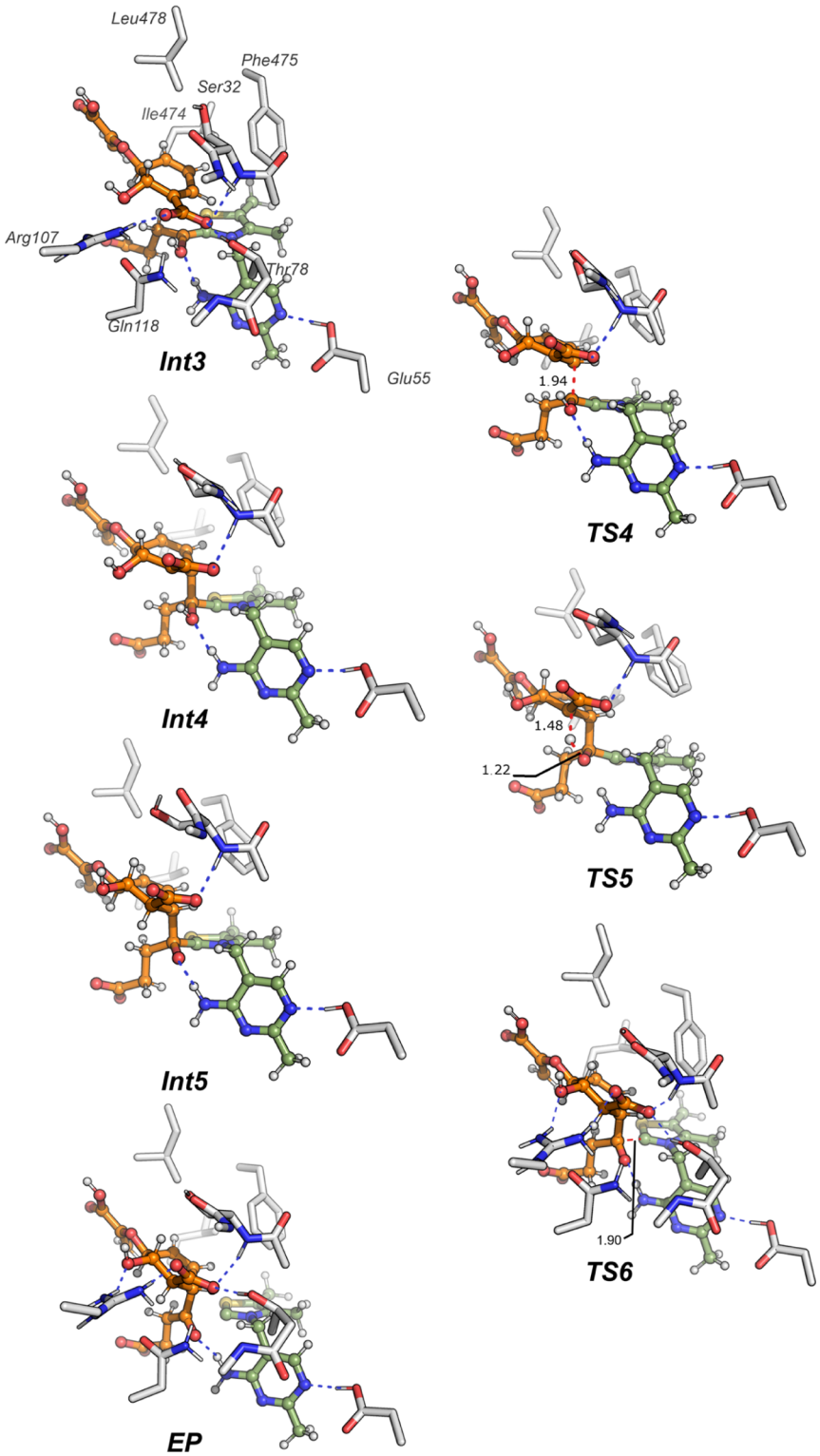

Figure 5. Optimized geometries of intermediates and transition states of the second half-reaction. For clarity, only a part of the active site model is shown in the figures. Note that the geometries of **TS6** and **EP** are derived from constrained optimizations, as discussed in the text.

The optimized geometries of the intermediates and TSs of the second half-reaction are shown in Figure 5, and the corresponding energy profile, with the energy of **Int3** set to zero, is provided in Figure 3.

The calculations show that if the reaction with IC proceeds directly from **Int2**, high energy barriers are observed for the subsequent steps (see Supporting Information). However, if the C2α-O alkoxide is protonated, thereby forming C2α-OH (as in **Int3**), lower barriers were found in the later steps. In these calculations, we have assumed that the proton comes from the bulk solvent (i.e., via **Path C**, Scheme 4), since there is no obvious proton source in the active site.

As mentioned above, the carbanion−enamine **Int2** and C2α-H forms of the Breslow intermediate **Int2-TdH**$^+$ are in

https://doi.org/10.1021/acscatal.1c02292
ACS Catal. 2021, 11, 12355−12366

Scheme 4. Formation of the Post-decarboxylation Tetrahedral Intermediate[a]

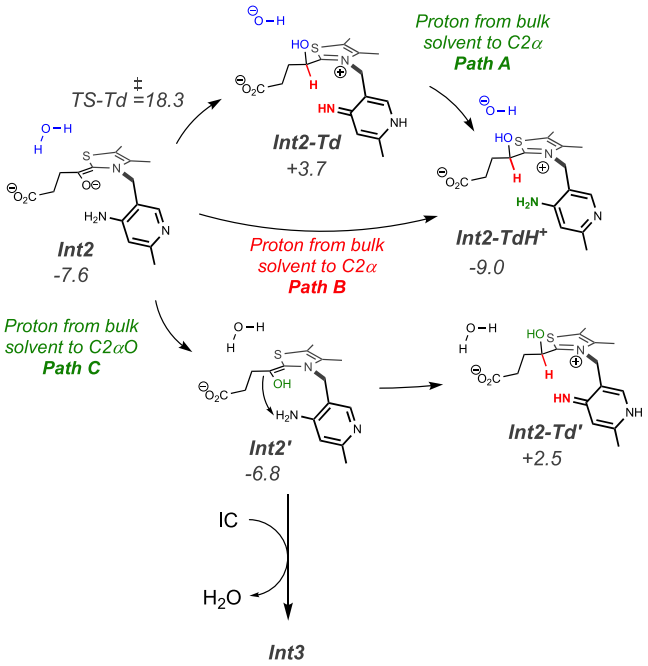

[a]Note that the formation of the **IP** form is accompanied by a proton transfer from Glu55 to N1′. The different colors indicate the different groups involved in the proton-transfer events of the various pathways. Energies (kcal/mol) are given relative to the starting **YI**.

equilibrium. Furthermore, the model of **Int2** shows that C2α and C2α-O are both poised for rapid proton transfer from N4′, and thus, it could be possible that **Int3** and **Int2-TdH**$^+$ can also interconvert via a proton exchange with the bulk solvent, as shown in Scheme 4.

From **Int3**, the reaction proceeds by the addition of the C2α carbanion to the β-carbon of IC (Scheme 3). The barrier for this step (**TS4**) is 5.8 kcal/mol and the resulting intermediate **Int4** is +2.5 kcal/mol relative to **Int3**. As seen from Scheme 3, **Int4** has two resonance forms, that is, a carbanion and an α-carboxylate dianion. The deviation from planarity of the carbon vicinal to the newly formed C−C bond (Figure 5) indicates that the carbanion form contributes to its reactivity.

Next, a proton is transferred from the C2α-OH group to the α-carbon of the acceptor (**TS5**). This process has a calculated barrier of 8.3 kcal/mol and affords **Int5** with a relative energy of −0.4 kcal/mol. **Int5** has some analogy with **Int1** in the first half-reaction in which the C2α-alkoxide is stabilized by a hydrogen bond with the N4′ amino group. Proton transfer from the N4′ amino group to the alkoxide provides **OC2**, a species in which the cofactor is in the **IP** form and whose energy is calculated to be very similar to that of **Int5**. This ready formation of **OC2** is again consistent with the observation that tetrahedral intermediates are accompanied by the formation of the **IP** state.[36,37]

It is important here to note that the addition of the enamine to the acceptor (**TS4**) and the subsequent protonation (**TS5**) take place on the same face of the acceptor, that is, in a relative *syn* disposition (see Figure 5). Protonation on the other face is not possible, as there are no ionizable residues on that face.

In the final step, **Int5** undergoes C−C bond cleavage to form the enzyme−product complex **EP**. Despite many efforts, the transition state for this step could not be located, as the geometry optimization always resulted in the (re)formation of **Int5**. Moreover, if the geometry of the **EP** complex was optimized, it too fell back to **Int5**. As a consequence, we sought an alternative means of estimating the energy barrier for this bond cleavage. To this end, we conducted a series of constrained optimizations, gradually increasing the distance of the scissile C2−C2α bond. The highest point in the series has an energy of ca. 7 kcal/mol relative to **Int3**. Using a similar approach, this time constraining the carbonyl group of the SEPHCHC product to be planar, the energy of the **EP** complex could be estimated to be ∼3 kcal/mol relative to **Int3**. Regardless of any error brought about by constraints in the geometry optimizations, these energies show that the final step is very feasible, with a very low barrier.

Close examination of the geometry of the constrained **EP** complex (Figure 5) sees that the region of SEPHCHC derived from IC is anchored in the active site by numerous hydrogen bonds to surrounding residues, such as Arg107, Thr78, and the backbone NHs of Ser32 and Arg33. At the same time, the succinyl side chain of SEPHCHC is bound to Arg395 and Arg413. The strength of these interactions is, presumably, the reason why the geometry of **EP** could not be optimized without constraints. Breaking all these interactions will undoubtedly be associated with a substantial energy penalty, one that could reasonably be expected to be higher than any other energy barrier found for the second half-reaction. On that basis, we predict that product release will be rate-determining for the second half-reaction.

3.4. Comparison of Computational and Experimental Results. Given the variety of assumptions and constraints involved, to assess the utility of the computational approach, it is incumbent upon us to compare the calculated energies (Figure 3) and structures (Figures 4 and 5) with available experimental data. Perhaps, the most obvious requirement is that calculations based on structures of native reaction intermediates will result in a product whose structure is consistent with that of the native product. Comfortingly, the calculations show that the enamine addition and the proton transfer to IC take place in a *syn* relative disposition. This results in the formation of the (1*R*,2*S*,5*S*,6*S*)-diastereoisomer of SEPHCHC obtained experimentally.[18] The same selectivity was observed for the addition of 2KG to the non-natural substrate (2*S*,3*S*)-2,3-dihydroxy-2,3-dihydrobenzoate (2,3-CHD) providing a product with (1*R*,5*S*,6*S*) stereochemistry.[45]

Since it provided the most informative structures, it is unfortunate that very little kinetic data are available for the *Mt*MenD isozyme. Fortunately, steady-state kinetic analyses have been carried out on wild-type and site-directed variants of both *Ec*MendD[21,23] and *Bs*MenD.[15] Since their active sites were almost identical, it was not surprising that the kinetic data were very similar, with apparent k_{cat} values of ∼20 min^{-1}, along with K_m values in the low micromolar range for 2KG, and the submicromolar range for IC. The active site of *Mt*MenD is virtually superimposable on those of the better characterized isozymes (see Supporting Information), so it is not unreasonable to expect the kinetic data to be comparable and that any conclusions drawn from models based on *Mt*MenD structures should be generally applicable.

In addition to the steady-state studies, the individual half-reactions of *Ec*MenD have been examined using pre-steady-state kinetics.[23] For the first half-reaction, it was concluded that the rate-determining step was associated with the binding of

https://doi.org/10.1021/acscatal.1c02292
ACS Catal. 2021, 11, 12355−12366

2KG, with a measured rate constant of 83.8 s^{-1}.[23] This corresponds to an energy barrier of ∼15 kcal/mol and serves as an upper limit for the first half-reaction. Although our calculations indicate that the decarboxylation step (**OC** → **TS2**) has the highest barrier, the calculated energy of 16.5 kcal/mol for the overall half-reaction is quite good agreement with the experimental value.

For the second half-reaction, product release was reported to be the slow step, although the possibility that the rate-determining formation of the **EP** complex could not be ruled out.[23] The measured rate constant, 0.3 s^{-1}, correlates well with steady-state k_{cat} values of 20 min^{-1} and implies a barrier of ∼18 kcal/mol, which is considerably higher than the 8.3 kcal/mol the calculations provide for the highest barrier of the second half-reaction (**Int3** → **TS5**). While, in themselves, these results may seem at odds, the fact that a much lower barrier was calculated for the chemical steps provides indirect evidence for the proposition that the release of the product from the active site is rate-limiting.[23] Moreover, the fact that **Int5**, identified in this work as the resting state of the second half-reaction, has been isolated and characterized crystallographically[18] lends additional credence to these calculations.

Ultimately, the aim of this work was to test the proposition that MenD operated by a novel mechanism, distinct from that of a canonical ThDP-dependent enzyme.[17,23] This hypothesis centered around the appearance of a tetrahedral hydroxysuccinyl ThDP adduct when crystals of MenD were soaked with 2KG in the absence of IC (**HSThDP**, Figure 1).[17−19,23] It was presumed that **HSThDP** was an intermediate formed by protonation of the carbanion−enamine formed by decarboxylation of the initial 2KG−ThDP adduct. Superficially, **HSThDP** was not dissimilar to tetrahedral post-decarboxylation intermediates/analogues found on other ThDP-dependent decarboxylases. However, the stereochemistry at C2α was such that the C2α−O pointed away from N4′, thereby preventing the typical intramolecular hydrogen bonding that promotes C2−C2α bond cleavage. The fact that **HSThDP** was found on wild-type *Mt*MenD,[18,19] as well as on wild-type and site-directed variants of *Ec*MenD,[17,23] indicated that it was not simply a crystallographic artifact and opened the possibility that it could play an important role in the MenD catalytic mechanism.

Although the overall structure of **HSThDP** was clear from the X-ray studies, the resolution of the structures was not sufficient to determine whether C2α was the carbanion or its C2α-hydroxyalkyl derivative.[17,18] Similarly, the protonation states of N1′ and N4′ were also uncertain,[17] so the initial assignments of these states were based primarily on CD spectra.[23] In the absence of IC and in the presence of saturating 2KG, the CD spectrum of *Ec*MenD showed a maximum around 303 nm and a broad minimum around 320−330 nm. The spectrum was unchanged even after 30 min. These bands are consistent with an equilibrium between the **IP** (imino) and **AP** (amino) forms of the cofactor, respectively.[34−36] Subsequently, pre-steady-state experiments showed that the formation of the signals occurred in two phases, a rapid increase in the positive signal at 302 nm followed by a slower decay with concomitant formation of a broad minimum at 320 nm. This was attributed to the initial rapid formation of the carbanion form of the post-decarboxylation intermediate followed by a slower conformational change to form the more stable **HSThDP**.[23] This slower change was not observed in the presence of high concentrations of IC. In light of these results, it was proposed that following decarboxylation of 2KG and protonation of C2α by N4′, an equilibrium was established between the neutral tetrahedral **HSThDP** and the planar carbanion/enamine. Additional evidence for the equilibrium came from experiments showing that C2α of **HSThDP** possessed an exchangeable proton and that the addition of IC to the *Ec*MenD/**HSThDP** complex gave rise to SEPHCHC.[17] The combined results led to the proposition of a novel mechanism in which **HSThDP** was a stable, on-pathway intermediate to be accumulated and used at low (i.e., nanomolar) concentrations of IC.[23]

The current calculations confirm that the formation of **HSThDP** is indeed possible but, rather than the **IP** state (i.e., **Int2-Td**, Scheme 4) suggested by Song et al.,[17] the cofactor adopts the **AP** state (i.e., **Int2-TdH**$^+$, Scheme 4). To explore this apparent contradiction, we first superposed the optimized structure of **Int2-TdH**$^+$ with the X-ray structure of the post-decarboxylation intermediate and found that the overall differences to be quite minor. Of these, perhaps the most important was the N4′-C2α distance of 3.0 Å observed in the X-ray structure and which had been used as secondary evidence in assigning the **IP** form to **HSThDP**. In **Int2-TdH**$^+$, this was found to be 3.4 Å. Subsequently, we performed a geometry optimization of **Int2-TdH**$^+$ in which the N4′-C2α distance was constrained to 3.0 Å. The results show that this structure is only 2 kcal/mol higher in energy than the unconstrained **Int2-TdH**$^+$ intermediate and still more than 10 kcal/mol more stable than the **IP** forms of **HSThDP**.

Overall, the calculations provide a viable pathway for an equilibrium mixture of **AP** and **IP** forms of the cofactor under steady-state conditions as well as the two-phased formation of **HSThDP** under pre-steady-state conditions. The rapid increase in the signal at 302 nm could stem from the formation of the pre-decarboxylation species **OC** (Scheme 3), in which the cofactor is in the **IP** state and whose formation is associated with low barriers. The subsequent slower decrease in ellipticity at 303 nm and concomitant formation of the broad minimum at around 320−330 nm would arise from the formation of **Int2-TdH**$^+$. Importantly, the similar energies of **OC** (−8.2 kcal/mol) and **Int2-TdH**$^+$ (−9.0 kcal/mol) are in line with the coexistence of the **AP** and **IP** forms of the cofactor under steady-state conditions.

While it could be argued that the assignments of **AP** and **IP** forms are merely semantic considerations, there is no doubt that the main tenet of the proposed noncanonical mechanism is that **HSThDP** will directly react with IC. Superposition of available X-ray structures of the *Mt*MenD−ThDP−IC ternary complex and the MenD−**HSThDP** complexes shows that although the conformation of the IC ring changes due to changes in bond hybridization, its overall position and most of its interactions change only marginally when **HSThDP** is formed (see Supporting Information).[18] This is consistent with the least motion mechanism found in BFDC and other ThDP-dependent enzymes.[32,33] Conversely, superposition of the experimental and calculated structures of **HSThDP** with the *Mt*MenD−ThDP−IC ternary complex showed that there were significant steric clashes between its C2α-O moiety of **HSThDP** and the acceptor (see Supporting Information). On this basis, it was apparent that if IC was present, neither **HSThDP** nor **Int2-TdH**$^+$could form without considerable movement of either the cofactor or other active-site residues. Similarly, IC could not bind if the tetrahedral intermediates were present. At a minimum, the binding affinity of IC would

https://doi.org/10.1021/acscatal.1c02292
ACS Catal. 2021, 11, 12355−12366

be considerably reduced. On this basis, it is highly unlikely that either **Int2-TdH**$^+$ or **HSThDP** (**Int2-Td**) is a catalytically active species. In fact, the only clearly viable scenario for the formation of SEPHCHC from **Int2-TdH**$^+$ requires the reformation of the enamine. As shown in Scheme 4, the formation of **Int2′** (which eventually leads to the formation of **Int3** upon binding of IC) from **Int2-TdH**$^+$ is thermodynamically feasible as the two species are of similar energy.

A comparison of computational and experimental results would not be complete without some discussion of the mechanistic roles of Arg395 and Arg413. A decade ago, mutagenesis showed that these two residues were important for catalysis.[16,21] More recently, X-ray structures have provided more detailed explanations of those results. In *Mt*MenD, for example, no movement of either arginine was observed when the substrate was bound,[18] indicative of a preorganized active site. Structures of site-directed *Ec*MenD variants showed that replacement of either Arg395 or Arg413 with alanine disrupted that site leading to both non-native binding of 2KG, as well as multiple conformations of the succinyl side chain of **HSThDP** and a concomitant reduction in catalytic activity.[46] The current calculations show that Arg395 and Arg413 interact with the carboxylate group of the succinyl moiety throughout the entire reaction pathway, which is consistent with all experimental data thus far reported. An interesting sidelight of the *Ec*MenD X-ray study was that one of the variants, R413A, exhibited only a small effect on 2KG binding and much greater effect on IC binding. The X-ray structure of R413A showed that the succinyl side chain of **HSThDP** adopted two different conformations, one of which protruded into the IC-binding site. Overall, this variant showed reduced binding affinity for both substrates but the reduction was significantly greater for IC. This observation lends support to the suggestion that the unfavorable interactions between the C2α-O moiety of **Int2Td/Int2Td-H**$^+$ and IC will result in an increase in the K_m value for the latter. The net result will be that nanomolar concentrations of IC will be less rather than more likely to bind to the **HSThDP/MenD** complex.

In summary, the present computational results support the proposition that the formation of **HSThDP** provides a viable mechanism to protect the reactive enamine. However, **HSThDP** will not react directly with **IC**; rather, it will revert to the enamine and thence to **Int3** before the reaction takes place.

4. CONCLUSIONS

We have used the quantum chemical-cluster approach to investigate the mechanism of the reaction catalyzed by MenD. Two models of the active site were constructed on the basis of the X-ray structures of the post-decarboxylation tetrahedral intermediate and the donor−acceptor adduct. These models were used to study the first and second halves of the reaction mechanism, respectively. The reaction mechanism obtained from the calculations is consistent with the previously reported kinetic measurements and provides new insights into the reactivity of MenD. For the first half-reaction, the decarboxylation step is associated with the highest barrier, while for the second half-reaction, all barriers are considerably lower than the estimated barrier for product release, therefore providing indirect evidence that the latter is the rate-determining step of the reaction. The mechanism is also consistent with the observed stereochemistry of the product, which requires that the enamine addition to the acceptor and the subsequent proton transfer from the donor to the acceptor both occur at the same face of the acceptor.

Overall, the calculations show that tetrahedral post-decarboxylation intermediate, **HSThDP**, observed in X-ray structures is indeed stable and is likely to be protonated at C2α. However, in contrast to previous reports, the calculations suggest that the cofactor is in the **AP** rather than **IP** state. Moreover, it cannot play any direct role on the reaction path, and the formation of **HSThDP** needs to be reversible to allow for the recovery of the enamine intermediate before the reaction can proceed. Thus, while **HSThDP** may provide a novel means by which the reactive carbanion intermediate is protected, the fundamental mechanism of MenD remains that of a canonical ThDP-dependent decarboxylase.

■ ASSOCIATED CONTENT

Supporting Information

The Supporting Information is available free of charge at https://pubs.acs.org/doi/10.1021/acscatal.1c02292.

Absolute energies and energy corrections for all species involved in the reaction mechanism, superpositions of structures, additional mechanistic results discussed in the text, and Cartesian coordinates of all structures (PDF)

■ AUTHOR INFORMATION

Corresponding Authors

Ferran Planas − *Department of Organic Chemistry, Arrhenius Laboratory, Stockholm University, Stockholm SE-10691, Sweden*; Email: ferran.padros@su.se

Fahmi Himo − *Department of Organic Chemistry, Arrhenius Laboratory, Stockholm University, Stockholm SE-10691, Sweden*; orcid.org/0000-0002-1012-5611; Email: fahmi.himo@su.se

Author

Michael J. McLeish − *Department of Chemistry and Chemical Biology, Indiana University-Purdue University Indianapolis, Indianapolis, Indiana 46202, United States*; orcid.org/0000-0002-9221-9119

Complete contact information is available at: https://pubs.acs.org/10.1021/acscatal.1c02292

Notes

The authors declare no competing financial interest.

■ ACKNOWLEDGMENTS

F.H. acknowledges financial support from the Swedish Research Council. Thanks to Prof. Frank Jordan (Rutgers University) and Prof. Kai Tittmann (University of Goettingen) for detailed discussions.

■ REFERENCES

(1) Meganathan, R. Biosynthesis of the Isoprenoid Quinones Menaquinone (Vitamin K2) and Ubiquinone (Coenzyme Q). *Escherichia coli and Salmonella typhimurium: Cellular and Molecular Biology*, 2nd ed.; American Society for Microbiology: Washington, DC, 1996; pp 642−656.

(2) Bhasin, M.; Billinsky, J. L.; Palmer, D. R. J. Steady-State Kinetics and Molecular Evolution of *Escherichia coli* MenD [(1R,6R)-2-Succinyl-6-Hydroxy-2,4-Cyclohexadiene-1-Carboxylate Synthase], an Anomalous Thiamin Diphosphate-Dependent Decarboxylase-Carboligase. *Biochemistry* **2003**, *42*, 13496−13504.

(3) Jiang, M.; Cao, Y.; Guo, Z.-F.; Chen, M.; Chen, X.; Guo, Z. Menaquinone Biosynthesis in *Escherichia coli*: Identification of 2-Succinyl-5-Enolpyruvyl-6-Hydroxy-3-Cyclohexene-1-Carboxylate as a Novel Intermediate and Re-Evaluation of MenD Activity. *Biochemistry* **2007**, *46*, 10979−10989.

(4) Jiang, M.; Chen, M.; Cao, Y.; Yang, Y.; Sze, K. H.; Chen, X.; Guo, Z. Determination of the Stereochemistry of 2-Succinyl-5-Enolpyruvyl-6-Hydroxy-3-Cyclohexene-1-Carboxylate, a Key Intermediate in Menaquinone Biosynthesis. *Org. Lett.* **2007**, *9*, 4765−4767.

(5) Jiang, M.; Chen, X.; Guo, Z.-F.; Cao, Y.; Chen, M.; Guo, Z. Identification and Characterization of (1*R*,6*R*)-2-Succinyl-6-Hydroxy-2,4- Cyclohexadiene-1-Carboxylate Synthase in the Menaquinone Biosynthesis of *Escherichia coli*. *Biochemistry* **2008**, *47*, 3426−3434.

(6) Kobayashi, K.; Ehrlich, S. D.; Albertini, A.; Amati, G.; Andersen, K. K.; Arnaud, M.; Asai, K.; Ashikaga, S.; Aymerich, S.; Bessieres, P.; Boland, F.; Brignell, S. C.; Bron, S.; Bunai, K.; Chapuis, J.; Christiansen, L. C.; Danchin, A.; Débarbouillé, M.; Dervyn, E.; Deuerling, E.; Devine, K.; Devine, S. K.; Dreesen, O.; Errington, J.; Fillinger, S.; Foster, S. J.; Fujita, Y.; Galizzi, A.; Gardan, R.; Eschevins, C.; Fukushima, T.; Haga, K.; Harwood, C. R.; Hecker, M.; Hosoya, D.; Hullo, M. F.; Kakeshita, H.; Karamata, D.; Kasahara, Y.; Kawamura, F.; Koga, K.; Koski, P.; Kuwana, R.; Imamura, D.; Ishimaru, M.; Ishikawa, S.; Ishio, I.; le Coq, D.; Masson, A.; Mauël, C.; Meima, R.; Mellado, R. P.; Moir, A.; Moriya, S.; Nagakawa, E.; Nanamiya, H.; Nakai, S.; Nygaard, P.; Ogura, M.; Ohanan, T.; O'Reilly, M.; O'Rourke, M.; Pragai, Z.; Pooley, H. M.; Rapoport, G.; Rawlins, J. P.; Rivas, L. A.; Rivolta, C.; Sadaie, A.; Sadaie, Y.; Sarvas, M.; Sato, T.; Saxild, H. H.; Scanlan, E.; Schumann, W.; Seegers, J. F. M. L.; Sekiguchi, J.; Sekowska, A.; Séror, S. J.; Simon, M.; Stragier, P.; Studer, R.; Takamatsu, H.; Tanaka, T.; Takeuchi, M.; Thomaides, H. B.; Vagner, V.; van Dijl, J. M.; Watabe, K.; Wipat, A.; Yamamoto, H.; Yamamoto, M.; Yamamoto, Y.; Yamane, K.; Yata, K.; Yoshida, K.; Yoshikawa, H.; Zuber, U.; Ogasawara, N. Essential *Bacillus subtilis* Genes. *Proc. Natl. Acad. Sci. U.S.A.* **2003**, *100*, 4678−4683.

(7) Akerley, B. J.; Rubin, E. J.; Novick, V. L.; Amaya, K.; Judson, N.; Mekalanos, J. J. A Genome-Scale Analysis for Identification of Genes Required for Growth or Survival of *Haemophilus influenzae*. *Proc. Natl. Acad. Sci. U.S.A.* **2002**, *99*, 966−971.

(8) Sassetti, C. M.; Boyd, D. H.; Rubin, E. J. Genes Required for Mycobacterial Growth Defined by High Density Mutagenesis. *Mol. Microbiol.* **2003**, *48*, 77−84.

(9) Debnath, J.; Siricilla, S.; Wan, B.; Crick, D. C.; Lenaerts, A. J.; Franzblau, S. G.; Kurosu, M. Discovery of Selective Menaquinone Biosynthesis Inhibitors against *Mycobacterium tuberculosis*. *J. Med. Chem.* **2012**, *55*, 3739−3755.

(10) Boersch, M.; Rudrawar, S.; Grant, G.; Zunk, M. Menaquinone Biosynthesis Inhibition: A Review of Advancements toward a New Antibiotic Mechanism. *RSC Adv.* **2018**, *8*, 5099−5105.

(11) For a selection of recent works in which 1,4-dicarbonyl compounds have been used as precursors, see: (a) Prasad, K. R.; Anbarasan, P. Enantiospecific Synthesis of (-)-Muricatacin from l-(+)-Tartaric Acid. *Tetrahedron: Asymmetry* **2006**, *17*, 2465−2467. (b) Handy, S.; Lavender, K. Organic Synthesis in Deep Eutectic Solvents: Paal-Knorr Reactions. *Tetrahedron Lett.* **2013**, *54*, 4377−4379. (c) Yin, G.; Wang, Z.; Chen, A.; Gao, M.; Wu, A.; Pan, Y. A New Facile Approach to the Synthesis of 3-Methylthio-Substituted Furans, Pyrroles, Thiophenes, and Related Derivatives. *J. Org. Chem.* **2008**, *73*, 3377−3383. (d) O'Reilly, E.; Iglesias, C.; Ghislieri, D.; Hopwood, J.; Galman, J. L.; Lloyd, R. C.; Turner, N. J. A Regio- and Stereoselective ω-Transaminase/Monoamine Oxidase Cascade for the Synthesis of Chiral 2,5-Disubstituted Pyrrolidines. *Angew. Chem.* **2014**, *126*, 2479−2482.

(12) Stetter, H. Catalyzed Addition of Aldehydes to Activated Double Bonds? A New Synthetic Approach. *Angew. Chem., Int. Ed.* **1976**, *15*, 639−647.

(13) Beigi, M.; Waltzer, S.; Zarei, M.; Müller, M. New Stetter Reactions Catalyzed by Thiamine Diphosphate Dependent MenD from *E. coli*. *J. Biotechnol.* **2014**, *191*, 64−68.

(14) Aleku, G. A.; Nowicka, B.; Turner, N. J. Biocatalytic Potential of Enzymes Involved in the Biosynthesis of Isoprenoid Quinones. *ChemCatChem* **2018**, *10*, 124−135.

(15) Dawson, A.; Fyfe, P. K.; Hunter, W. N. Specificity and Reactivity in Menaquinone Biosynthesis: The Structure of *Escherichia coli* MenD (2-Succinyl-5-Enolpyruvyl-6-Hydroxy-3-Cyclohexadiene-1-Carboxylate Synthase). *J. Mol. Biol.* **2008**, *384*, 1353−1368.

(16) Dawson, A.; Chen, M.; Fyfe, P. K.; Guo, Z.; Hunter, W. N. Structure and Reactivity of *Bacillus subtilis* MenD Catalyzing the First Committed Step in Menaquinone Biosynthesis. *J. Mol. Biol.* **2010**, *401*, 253−264.

(17) Song, H.; Dong, C.; Qin, M.; Chen, Y.; Sun, Y.; Liu, J.; Chan, W.; Guo, Z. A Thiamine-Dependent Enzyme Utilizes an Active Tetrahedral Intermediate in Vitamin K Biosynthesis. *J. Am. Chem. Soc.* **2016**, *138*, 7244−7247.

(18) Jirgis, E. N. M.; Bashiri, G.; Bulloch, E. M. M.; Johnston, J. M.; Baker, E. N. Structural Views along the *Mycobacterium tuberculosis* MenD Reaction Pathway Illuminate Key Aspects of Thiamin Diphosphate-Dependent Enzyme Mechanisms. *Structure* **2016**, *24*, 1167−1177.

(19) Bashiri, G.; Nigon, L. V.; Jirgis, E. N. M.; Ho, N. A. T.; Stanborough, T.; Dawes, S. S.; Baker, E. N.; Bulloch, E. M. M.; Johnston, J. M. Allosteric Regulation of Menaquinone (Vitamin K2) Biosynthesis in the Human Pathogen *Mycobacterium tuberculosis*. *J. Biol. Chem.* **2020**, *295*, 3759−3770.

(20) (a) Priyadarshi, A.; Saleem, Y.; Nam, K. H.; Kim, K.-S.; Park, S.-Y.; Kim, E. E.; Hwang, K. Y. Structural Insights of the MenD from *Escherichia coli* Reveal ThDP Affinity. *Biochem. Biophys. Res. Commun.* **2009**, *380*, 797−801. (b) Priyadarshi, A.; Kim, E. E.; Hwang, K. Y. Structural and Functional Analysis of Vitamin K2 Synthesis Protein MenD. *Biochem. Biophys. Res. Commun.* **2009**, *388*, 748−751.

(21) Fang, M.; Macova, A.; Hanson, K. L.; Kos, J.; Palmer, D. R. J. Using Substrate Analogues to Probe the Kinetic Mechanism and Active Site of *Escherichia coli* MenD. *Biochemistry* **2011**, *50*, 8712−8721.

(22) Wille, G.; Meyer, D.; Steinmetz, A.; Hinze, E.; Golbik, R.; Tittmann, K. The Catalytic Cycle of a Thiamin Diphosphate Enzyme Examined by Cryocrystallography. *Nat. Chem. Biol.* **2006**, *2*, 324−328.

(23) Qin, M.; Song, H.; Dai, X.; Chan, C. K.; Chan, W.; Guo, Z. Single-Turnover Kinetics Reveal a Distinct Mode of Thiamine Diphosphate-Dependent Catalysis in Vitamin K Biosynthesis. *ChemBioChem* **2018**, *19*, 1514−1522.

(24) Planas, F.; Sheng, X.; McLeish, M. J.; Himo, F. A Theoretical Study of the Benzoylformate Decarboxylase Reaction Mechanism. *Front. Chem.* **2018**, *6*, 205.

(25) Planas, F.; McLeish, M. J.; Himo, F. Computational Characterization of Enzyme-Bound Thiamin Diphosphate Reveals a Surprisingly Stable Tricyclic State: Implications for Catalysis. *Beilstein J. Org. Chem.* **2019**, *15*, 145−159.

(26) Planas, F.; McLeish, M. J.; Himo, F. Computational Study of Enantioselective Carboligation Catalyzed by Benzoylformate Decarboxylase. *ACS Catal.* **2019**, *9*, 5657−5667.

(27) (a) Becke, A. D. Density-functional thermochemistry. III. The Role of Exact Exchange. *J. Chem. Phys.* **1993**, *98*, 5648−5652. (b) Lee, C.; Yang, W.; Parr, R. G. Development of the Colle-Salvetti Correlation-Energy Formula into a Functional of the Electron Density. *Phys. Rev. B: Condens. Matter Mater. Phys.* **1988**, *37*, 785−789. (c) Grimme, S.; Antony, J.; Ehrlich, S.; Krieg, H. A Consistent and Accurate *ab initio* Parametrization of Density Functional Dispersion Correction (DFT-D) for the 94 Elements H-Pu. *Chem. Phys.* **2010**, *132*, 154104. (d) Grimme, S.; Ehrlich, S.; Goerigk, L. Effect of the Damping Function in Dispersion Corrected Density Functional Theory. *J. Comput. Chem.* **2011**, *32*, 1456−1465.

(28) Frisch, M. J.; Trucks, G. W.; Schlegel, H. B.; Scuseria, G. E.; Robb, M. A.; Cheeseman, J. R.; Scalmani, G.; Barone, V.; Mennucci, B.; Petersson, G. A.; Nakatsuji, H.; Caricato, M.; Li, X.; Hratchian, H. P.; Izmaylov, A. F.; Bloino, J.; Zheng, G.; Sonnenberg, J. L.; Hada, M.; Ehara, M.; Toyota, K.; Fukuda, R.; Hasegawa, J.; Ishida, M.; Nakajima, T.; Honda, Y.; Kitao, O.; Nakai, H.; Vreven, T.;

Montgomery, J. A., Jr.; Peralta, J. E.; Ogliaro, F.; Bearpark, M.; Heyd, J. J.; Brothers, E.; Kudin, K. N.; Staroverov, V. N.; Keith, T.; Kobayashi, R.; Normand, J.; Raghavachari, K.; Rendell, A.; Burant, J. C.; Iyengar, S. S.; Tomasi, J.; Cossi, M.; Rega, N.; Millam, J. M.; Klene, M.; Knox, J. E.; Cross, J. B.; Bakken, V.; Adamo, C.; Jaramillo, J.; Gomperts, R.; Stratmann, R. E.; Yazyev, O.; Austin, A. J.; Cammi, R.; Pomelli, C.; Ochterski, J. W.; Martin, R. L.; Morokuma, K.; Zakrzewski, V. G.; Voth, G. A.; Salvador, P.; Dannenberg, J. J.; Dapprich, S.; Daniels, A. D.; Farkas, O.; Foresman, J. B.; Ortiz, J. V.; Cioslowski, J.; Fox, D. J. *Gaussian 09*, Revision D.01; Gaussian, Inc.: Wallingford CT, 2013.

(29) For recent reviews, see: (a) Sheng, X.; Himo, F. Mechanisms of Metal-Dependent Non-Redox Decarboxylases from Quantum Chemical Calculations. *Comput. Struct. Biotechnol. J.* **2021**, *19*, 3176−3186. (b) Sheng, X.; Kazemi, M.; Planas, F.; Himo, F. Modeling Enzymatic Enantioselectivity using Quantum Chemical Methodology. *ACS Catal.* **2020**, *10*, 6430−6449. (c) Himo, F. Recent Trends in Quantum Chemical Modeling of Enzymatic Reactions. *J. Am. Chem. Soc.* **2017**, *139*, 6780−6786. (d) Blomberg, M. R. A.; Borowski, T.; Himo, F.; Liao, R.-Z.; Siegbahn, P. E. M. Quantum Chemical Studies of Mechanisms for Metalloenzymes. *Chem. Rev.* **2014**, *114*, 3601−3658.

(30) Marenich, A. V.; Cramer, C. J.; Truhlar, D. G. Universal Solvation Model Based on Solute Electron Density and on a Continuum Model of the Solvent Defined by the Bulk Dielectric Constant and Atomic Surface Tensions. *J. Phys. Chem. B* **2009**, *113*, 6378−6396.

(31) (a) Lind, M. E. S.; Himo, F. Theoretical Study of Reaction Mechanism and Stereoselectivity of Arylmalonate Decarboxylase. *ACS Catal.* **2014**, *4*, 4153−4160. (b) Sheng, X.; Lind, M. E. S.; Himo, F. Theoretical Study of the Reaction Mechanism of Phenolic Acid Decarboxylase. *FEBS J.* **2015**, *282*, 4703−4713. (c) Sheng, X.; Zhu, W.; Huddleston, J.; Xiang, D. F.; Raushel, F. M.; Richards, N. G. J.; Himo, F. A Combined Experimental-Theoretical Study of the LigW-Catalyzed Decarboxylation of 5-Carboxyvanillate in the Metabolic Pathway for Lignin Degradation. *ACS Catal.* **2017**, *7*, 4968−4974.

(32) Schütz, A.; Golbik, R.; König, S.; Hübner, G.; Tittmann, K. Intermediates and Transition States in Thiamin Diphosphate-Dependent Decarboxylases. A Kinetic and NMR Study on Wild-Type Indolepyruvate Decarboxylase and Variants Using Indolepyruvate, Benzoylformate, and Pyruvate as Substrates. *Biochemistry* **2005**, *44*, 6164−6179.

(33) Bruning, M.; Berheide, M.; Meyer, D.; Golbik, R.; Bartunik, H.; Liese, A.; Tittmann, K. Structural and Kinetic Studies on Native Intermediates and an Intermediate Analogue in Benzoylformate Decarboxylase Reveal a Least Motion Mechanism with an Unprecedented Short-Lived Predecarboxylation Intermediate. *Biochemistry* **2009**, *48*, 3258−3268.

(34) Nemeria, N. S.; Chakraborty, S.; Balakrishnan, A.; Jordan, F. Reaction Mechanisms of Thiamin Diphosphate Enzymes: Defining States of Ionization and Tautomerization of the Cofactor at Individual Steps. *FEBS J.* **2009**, *276*, 2432−3446.

(35) Nemeria, N.; Binshtein, E.; Patel, H.; Balakrishnan, A.; Vered, I.; Shaanan, B.; Barak, Z. e.; Chipman, D.; Jordan, F. Glyoxylate Carboligase: A Unique Thiamin Diphosphate-Dependent Enzyme That Can Cycle between the 4′-Aminopyrimidinium and 1′,4′-Iminopyrimidine Tautomeric Forms in the Absence of the Conserved Glutamate. *Biochemistry* **2012**, *51*, 7940−7952.

(36) Nemeria, N.; Baykal, A.; Joseph, E.; Zhang, S.; Yan, Y.; Furey, W.; Jordan, F. Tetrahedral Intermediates in Thiamin diphosphate-Dependent Decarboxylations Exist as a 1′,4′-Imino Tautomeric Form of the Coenzyme, Unlike the Michaelis Complex or the Free Coenzyme. *Biochemistry* **2004**, *43*, 6565−6575.

(37) Nemeria, N.; Chakraborty, S.; Baykal, A.; Korotchkina, L. G.; Patel, M. S.; Jordan, F. The 1′,4′-Iminopyrimidine Tautomer of Thiamin Diphosphate Is Poised for Catalysis in Asymmetric Active Centers on Enzymes. *Proc. Natl. Acad. Sci. U.S.A.* **2007**, *104*, 78−82.

(38) Tittmann, K.; Wille, G. X-ray Crystallographic Snapshots of Reaction Intermediates in Pyruvate Oxidase and Transketolase Illustrate Common Themes in Thiamin Catalysis. *J. Mol. Catal. B: Enzym.* **2009**, *61*, 94−99.

(39) Jaña, G. A.; Delgado, E. J. Electron Density Reactivity Indexes of the Tautomeric/Ionization Forms of Thiamin Diphosphate. *J. Mol. Model.* **2013**, *19*, 3799−3803.

(40) Zhang, J.; Liu, Y. Theoretical Study of the Catalytic Mechanism of Glyoxylate Carboligase and Its Mutant V51E. *Theor. Chem. Acc.* **2017**, *136*, 1−15.

(41) Zhang, J.; Sheng, X.; Hou, Q.; Liu, Y. Theoretical Investigation on the Dissociation of (R)-Benzoin Catalyzed by Benzaldehyde Lyase. *Int. J. Quantum Chem.* **2014**, *114*, 375−382.

(42) Hou, Q.; Gao, J.; Liu, Y.; Liu, C. A QM/MM Study on the Catalytic Mechanism of Pyruvate Decarboxylase. *Theor. Chem. Acc.* **2012**, *131*, 1280.

(43) Wang, J.; Dong, H.; Li, S.; He, H. Theoretical Study toward Understanding the Catalytic Mechanism of Pyruvate Decarboxylase. *J. Phys. Chem. B* **2005**, *109*, 18664−18672.

(44) Sheng, X.; Liu, Y.; Zhang, R. A Theoretical Study of the Catalytic Mechanism of Oxalyl-CoA Decarboxylase, an Enzyme for Treating Urolithiasis. *RSC Adv.* **2014**, *4*, 35777−35788.

(45) Schapfl, M.; Baier, S.; Fries, A.; Ferlaino, S.; Waltzer, S.; Müller, M.; Sprenger, G. A. Extended Substrate Range of Thiamine Diphosphate-Dependent MenD Enzyme by Coupling of Two C−C-Bonding Reactions. *Appl. Microbiol. Biotechnol.* **2018**, *102*, 8359−8372.

(46) Qin, M.; Song, H.; Dai, X.; Chen, Y.; Guo, Z. Two Active Site Arginines Are Critical Determinants of Substrate Binding and Catalysis in MenD: A Thiamine-Dependent Enzyme in Menaquinone Biosynthesis. *Biochem. J.* **2018**, *475*, 3651−3667.

https://doi.org/10.1021/acscatal.1c02292
ACS Catal. 2021, 11, 12355−12366